Clays and Clay Minerals, Vol. 37, No. 3, 219–226, 1989.

CLAY-ORGANIC COMPLEXES AS A CEMENTING AGENT IN THE ARAHAMA SAND DUNE, JAPAN

KAZUE TAZAKI,[1] S. KIMURA,[2] T. YOSHIMURA,[3] J. AKAI,[3] and W. S. FYFE[4]

[1] Department of Geology, Shimane University, Nishikawatsu
Matsue, Shimane 690, Japan

[2] Toyosaka High School, Toyosaka, Niigata 950-33, Japan

[3] Department of Geology and Mineralogy, Niigata University
Ikarashi, Niigata 950-21, Japan

[4] Department of Geology, University of Western Ontario
London, Ontario, N6A 5B7, Canada

Abstract—*Cementing materials in the* Arahama sand dune, Japan, were studied mineralogically and biogeochemically to gain a better understanding of the cause of hardening. The cementing material is a clay-organic complex composed of noncrystalline gels and a matrix of small, poorly crystalline particles showing 14–16-Å spacings. The gel materials appear to have transformed into the poorly crystalline particles, which have a high carbon content and Al/Si ratios of 2.2 to 2.0. These particles are slightly richer in Si and poorer in Fe than the gel materials themselves. The organic portion of the complex can be removed by H_2O_2 treatment, leaving a noncrystalline network-structure containing a dispersed granular component. Scanning auger-depth profiles of individual particles show a high surface concentration of C and O and an increase in the Al/Si ratio with depth. The energy-intensity distribution suggests a mixture of carbon compounds having a major core-line binding energy of a hydrocarbon. The gel-cementing materials in the sand dune may have been formed from biochemical weathering products of organic matter, which subsequently controlled the formation of clay-organic complexes.

要旨ー柏崎海岸の荒浜砂丘を構成する砂丘砂は固結している。その原因を解明するため、セメント物質を鉱物学的・生地球化学的に研究した。セメント物質は非晶質ゲルと１４－１６Åの面間隔をもつ低結晶度の小粒子からなる粘土－有機複合体であることが明かとなった。小粒結晶はゲル物質から形成され、その炭素含有量は高く、Ａｌ／Ｓｉ比は２．２－２．０である。ゲル物質と比べると、Ｓｉはわずかに多く、Ｆｅが少ない。複合体の有機質部分をH_2O_2処理により除去すると、粒状の部分が散在する非晶質物質のネットワーク構造が残る。走査オージェ奥行プロファイルはＣとＯの表面への濃集を示し、深さとともにＡｌ／Ｓｉ比が増加することを示した。エネルギー強度分布は炭化水素の主要のσ結合エネルギーをもつ炭素化合物の特徴を示す。砂丘砂のゲル状セメント物質は、粘土－有機複合体の形成をコントロールした有機物の生化学的風化作用によって生じたものである。

Key Words—Cementing agent, Clay-organic complex, Gel, Sand dune, Scanning auger multiprobe analysis, Transmission electron microscopy, X-ray photoelectron spectroscopy.

INTRODUCTION

A gel-cementing material has been identified in the Arahama sand dune, Niigata, Japan. The cementing material coexists with clay-organic complexes and together have formed a hard mass of sand particles. Considerable research has been devoted to the study of the formation of coating and cementing materials in sandy soils, rocks, and minerals. Fungi (Bond and Harris, 1964), noncrystalline mucilaginous coatings with bacteria (Berthelin and Munier-Lamy, 1983), mycelial filaments (Spyridakis *et al.*, 1967), imogolite (Research Group of Harden Sand, 1984; Tazaki, 1979, 1980), gibbsite (Niigata Ancient Dune Research Group, 1967), and ultra-thin Cu-S films (Tazaki *et al.*, 1988) have been reported.

Little work has been carried out on the geochemical behavior of the cementing agents using micro-analytical surface techniques, and the gel cementing material itself has previously not been characterized. In the present study, geochemical, biochemical, and mineralogical properties of the cementing agents were obtained using X-ray powder diffractometry (XRD), scanning electron microscopy (SEM), transmission electron microscopy (TEM) with energy dispersive X-ray spectrometer (EDX), scanning auger multiprobe (SAM), and X-ray photoelectron spectroscopy (XPS). The mineral nature of the cementing materials was evaluated by XRD; SEM-EDX, TEM-EDX, and XPS were used to determine elemental distributions; and depth profile of surface analyses were made by SAM and XPS. The mineralogy of individual particle was determined by TEM-EDX and selected-area electron diffraction (SAD).

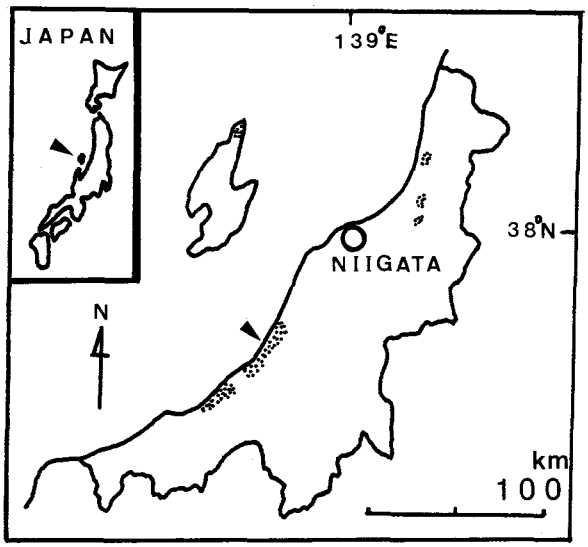

Figure 1. Map of the sample localities, Niigata, Japan. Gel cementing materials were collected from the Arahama sand dune (dotted area).

EXPERIMENTAL

Samples

The gel cementing materials were collected from the Arahama sand dune, which forms a part of the Niigata coastal sand dune distributed along the Sea of Japan (arrow in Figure 1). The Arahama sand dune is composed of overlying Holocene dune and underlying Pleistocene dune near the present seashore. The sampling point is located about 500 m from the shore where only the Pleistocene dune is found.

The Pleistocene dune is divided into two sand beds by an intercalated brown soil at the sampling point. The upper bed is the Yukinari sand bed and the lower bed is the Banjin sand bed (Figure 2). The upper brown soil is more advanced in soil formation than the intercalated brown soil. The Yukinari sand bed consists of yellow-brown, well-sorted, medium-unconsolidated sand grains and is easily crumbled. The thickness of the sand bed is about 4 m. The Banjin sand bed consists of grey, well-sorted medium-consolidated sand grains and is divisible into two parts. The upper part is massive, whereas the lower part contains intercalated thin clay layers and shows parallel lamination. Extensive cracks and minor faults exist throughout the bed and are coated with films of gibbsite. Therefore, the Banjin sand bed has a tendency to break easily into blocks if it is dry.

Gel cementing materials occur in the intercalated brown soil and in the upper part of the Banjin sand bed. They are especially abundant in the lower half of the brown soil and within the uppermost meter of the Banjin sand bed. They are visible to the naked eyes on outcrops.

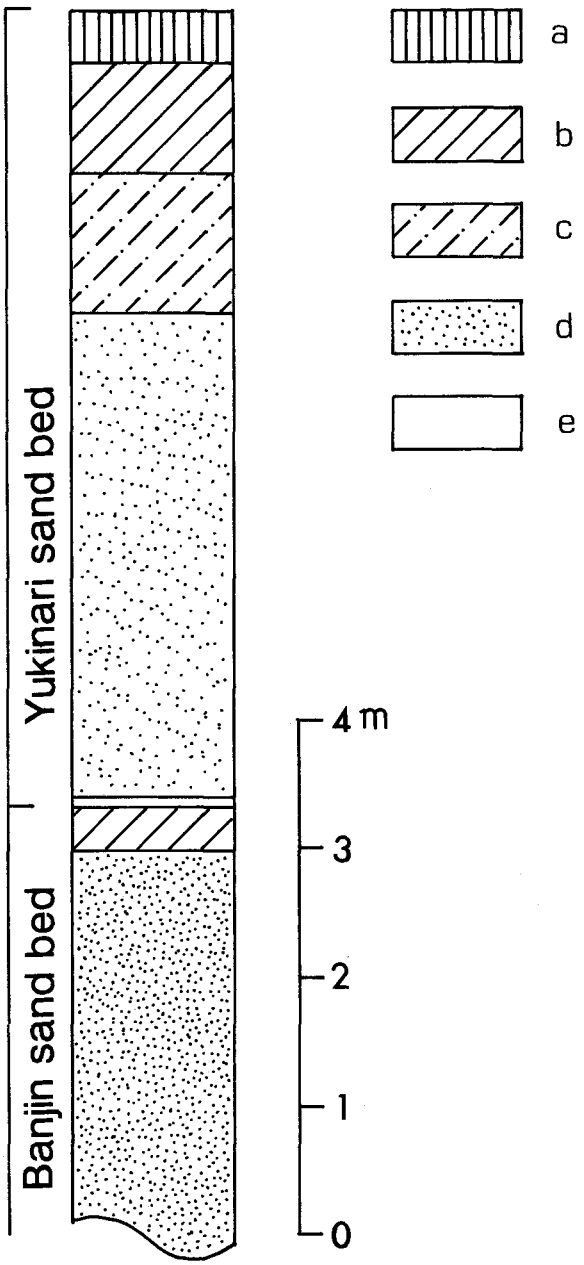

Figure 2. Columnar section at the sampling point. a. black humic soil, b. brown soil, c. sandy brown soil, d. dune sands, e. white clay.

Methods

Gel cementing materials were ground under water in a porcelain mortar; the resulting finest fraction was then decanted, and the suspension was allowed to settle. After about 0.5 h the supernatant suspension was pipeted and sedimented onto a glass slide. The samples were examined by XRD with a Rigaku goniometer using CuKα radiation and operated at 40 kV and 20 mA. Using a <2-μm size fraction, XPS analyses were

https://doi.org/10.1346/CCMN.1989.0370304 Published online by Cambridge University Press

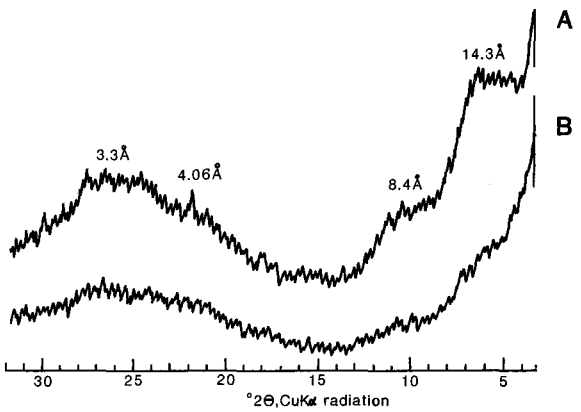

Figure 3. X-ray powder diffraction pattern of gel cementing material. (A) no treatment, (B) treatment with H_2O_2.

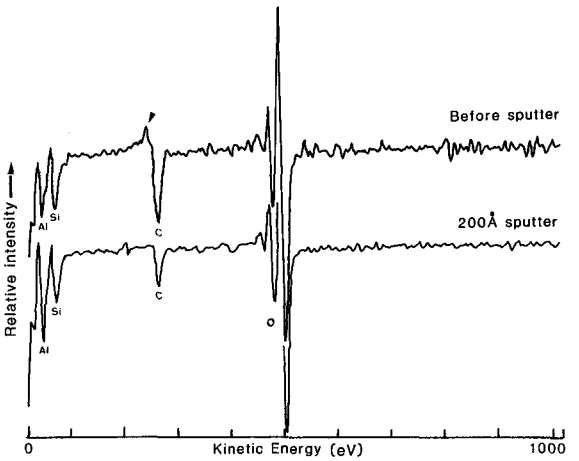

Figure 5. High-resolution scanning auger multiprobe depth-profile of gel cementing material. Arrow shows presence of hump before sputter.

conducted using a UHV, SSX-100 X-ray photoelectron spectrometer equipped with a custom-designed vacuum system and sample treatment chamber. Air-dried samples were mounted on Ni grids and desiccated before being inserted into the high vacuum chamber of the spectrometer. A monochromatized AlKα X-ray exciting beam was used, and specimen charging was controlled with a low-energy electron flood gun. All binding energies were referenced to C (1s) at 285.0 eV. Spot sizes were 1000, 600, and 300 μm in diameter for whole spectra, depth profile, and high resolution of carbon, respectively.

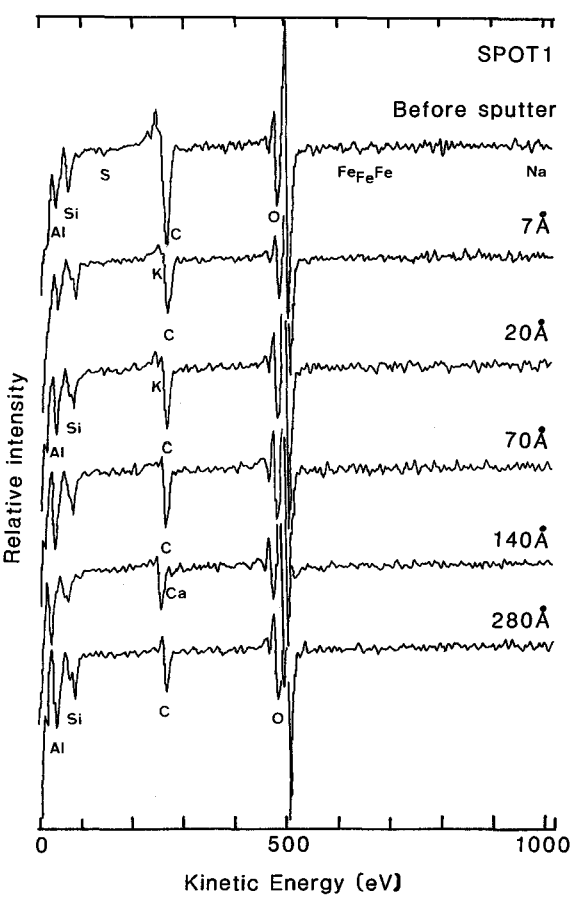

Figure 4. Scanning auger multiprobe depth-profile analyses of the surface composition of gel cementing material (spot 1). Sample was mounted on indium foil and sputtered with Ar^+.

Using a <2-μm size fraction, SAM analyses were carried out with a Perkin-Elmer Physical Electronics model 600 instrument, using an accelerating voltage of 3 kV and an electron beam 1 μm in diameter. The indium foil containing the embedded air-dried samples was mounted on the standard carousel and sputtered by 2-keV Ar^+ at a rate of 70-Å/min for depth profiles. Graphite was used for comparison with carbon in the gel cementing materials.

SEM-EDX was carried out with an ISI DS-130 SEM coupled with a PGT System III EDX at accelerating voltages of 30 kV. Grains (<2 μm) were concentrated by the sedimentation technique described above and pipeted onto grids for transmission electron microscopy. The instrument used was either a JEOL-EM 100C or a Philips EM 400T instrument equipped with EDX. Both instruments were operated at 100 kV with a liquid-nitrogen-cooled anticontamination device in place at all times. EDX was conducted using electron beam spot sizes of about 2000 Å, and counts were collected for 100 s (live time). SAD patterns were calibrated using a Au standard.

RESULTS

X-ray powder diffraction

The XRD trace of the gel cementing material (<2 μm) from 3° to 32°2θ (Figure 3) shows the presence of three broad peaks at about 14.3, 8.4, and 3.3 Å. The 14.3- and 8.4-Å peaks were destroyed by heating the sample at 300°C, and only the 3.3-Å peak remained. The XRD data are similar to those reported for imo-

https://doi.org/10.1346/CCMN.1989.0370304 Published online by Cambridge University Press

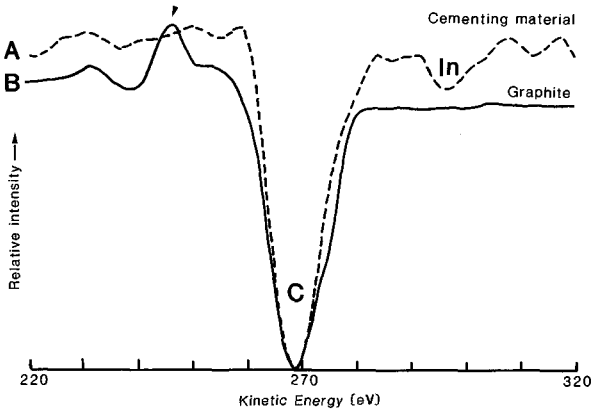

Figure 6. High-resolution scanning auger multiprobe analyses of (A) gel cementing material and (B) graphite for comparison of carbon peaks.

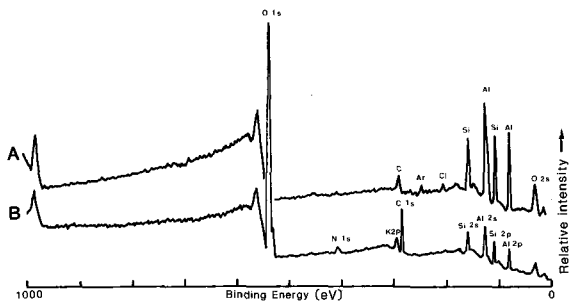

Figure 7. X-ray photoelectron spectra of gel cementing material (B) before and (A) after sputter showing a lower concentration of carbon and a higher Al/Si ratio after a 150-Å sputter.

golite (Wada, 1977). Opaline silica or cristobalite (d = 4.06 Å) appears to be a trace component of the sample, whereas imogolite-like minerals and noncrystalline materials are major components. The nature of noncrystalline materials and traces of clay minerals are difficult to determine by XRD, but the TEM, SAM, and XPS data confirm the presence of organic matter and a noncrystalline aluminosilicate. The XRD pattern for a sample from which organic matter was removed by H_2O_2 treatment is shown in Figure 3B. The 14.3- and 8.4-Å peaks were destroyed by the H_2O_2 treatment, suggesting that imogolite was not present.

Scanning auger multiprobe analysis

SAM was used to determine the surface chemistry of the gel cementing materials. Auger sputtering was performed on few spots to obtain compositional depth profiles. Figure 4 shows a high surface concentration of C and O and an increase of the Al/Si ratio with depth. The Al/Si ratio before sputter was 1, whereas after a 280-Å sputter, the ratio was 2. Trace amounts of S, K, Ca, Fe, and Na were also recognized. Iron was present at the top of the surface (i.e., in the outermost portion of the grain) and was removed after a 7-Å sputter. The carbon peak remained after a 280-Å sputter, but the intensity of the peak decreased to less than half. The remaining C component suggests the presence of organic matter. With increasing depth, the carbon intensity decreased rapidly, suggesting the presence of an atmospheric hydrocarbon coating on the surface. The Si peak appears to have separated into two peaks with increasing depth, suggesting a change in the structural environment of the Si.

To characterize the carbon-rich surface in more detail, SAM observation was used, as shown in Figure 5. The main carbon peak was recognized at 270 eV on surfaces before and after a 200-Å sputter. A small hump next to the main carbon peak (arrow, Figure 5) on the surface before sputter was most likely due to adventitious atmospheric hydrocarbon contamination. High-resolution SAM observations were obtained on the gel cementing material (A) and standard graphite (B) for a comparison of the carbon peaks (Figure 6). A small carbon peak at 245 eV (arrow) was noted next to the main broad carbon peak at 268 eV in the graphite. The cementing material showed only a narrow carbon peak at 268 eV. The In peak was due to the embedded indium foil. The SAM data suggest the presence of soil organic carbon in the gel cementing materials.

X-ray photoelectron spectroscopy

The XPS spectra of the gel cementing material are shown in Figure 7. The spectrum (A) after a 150-Å sputter showed a lower concentration of carbon and a higher Al/Si ratio than those of spectrum (B) before sputter. Both spectra were obtained using a 1000-μm diameter beam. Bulk samples showed not only O, C, Al, and Si peaks, but also small peaks of N and K.

A more detailed calculation of the carbon content and the Al/Si ratio using the XPS technique (600-μm beam diameter) showed that the C (1s) decreased to 6 atom % at 150-Å depth from 11 atom % on the surface. The Al/Si ratio was calculated to be 1.7 after a 150-Å sputter (Table 1). The quantity and nature of the carbon was investigated by high-resolution XPS using a beam diameter of 300 μm (Figure 8). The energy-intensity distribution was characteristic of a mixture of carbon compounds having a major core-line binding energy at 285.3 eV (83.7%) and minor components at 286.5 eV (10.9%) and 288.8 eV (5.4%). The three binding energies were identified as hydrocarbon (CH_2) at 285.3 eV, amine ($C–NH_2$) at 286.5 eV, and carbonate (CO_3) at 288.9 eV. The energies at 286.5 and 288.8 eV is probably due to a chemisorbed species (i.e., organic matter) and a chelate complex with Al, whereas the energy at 285.3 eV is probably due to atmospheric contamination (Clark *et al.*, 1978).

Scanning electron microscopy

A typical SEM of the air-dried sample is shown in Figure 9A. The samples are closely packed and have

https://doi.org/10.1346/CCMN.1989.0370304 Published online by Cambridge University Press

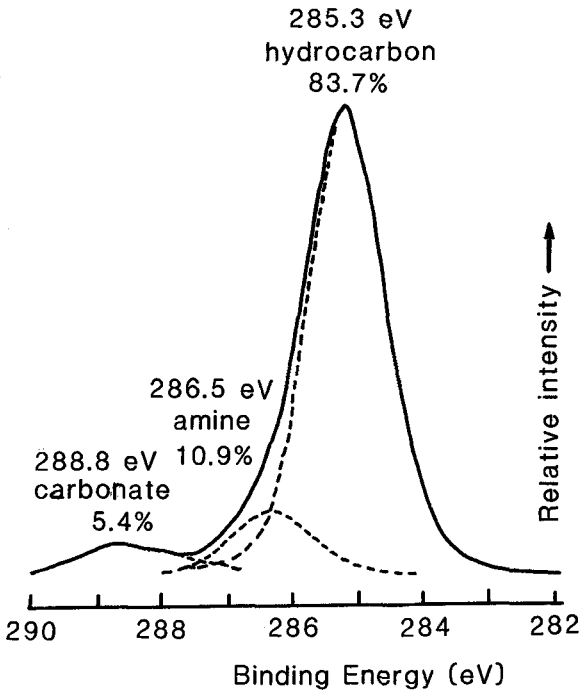

Figure 8. High-resolution X-ray photoelectron carbon pattern of gel cementing material showing mixture of carbon compounds.

a high porosity (Figure 9B), even though TEMs of the water suspensions show a network texture. Several minor element impurities in the bulk sample were detected by EDX (Figure 9C). The particles showed not only Al and Si peaks, but also small peaks of Cl, K, Ca, and Fe. The Al/Si ratios detected by EDX agreed with the SAM and XPS results.

Transmission electron microscopy

Using a <2-μm size fraction, the TEM examination of water suspensions of the cementing materials revealed the presence of noncrystalline gel network and a matrix of small, poorly crystalline particles. The net-

Table 1. Chemical analyses of cementing materials (B) before and (A) after sputter using X-ray photoelectron spectrometer.

Element	Atom % A	Atom % B
O 1s	49.10	47.51
N 1s	—	1.73
C 1s	5.93	11.17
Si 2s	—	9.07
Al 2s	29.70	16.87
Si 2p	14.14	9.97
Al 2p	—	3.68
Cl 2p	1.13	—
Total	100.00	100.00

A = at 150-Å depth; B = no sputter.

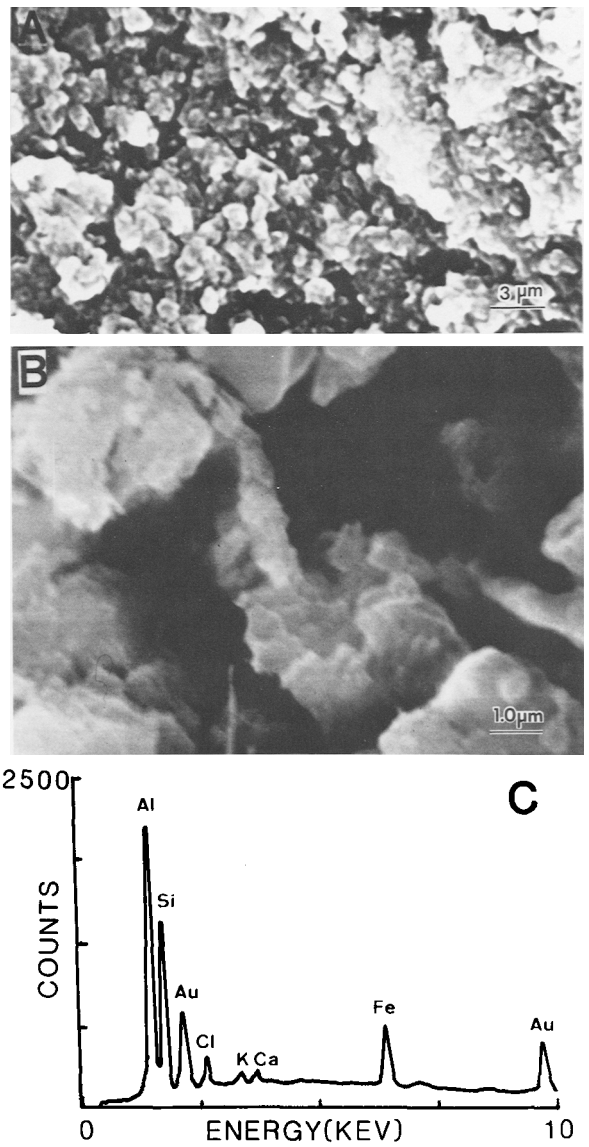

Figure 9. (A and B) Scanning electron micrographs of the air-dried gel cementing material showing packed aggregates with high porosity, (C) energy dispersive X-ray spectra showing aluminosilicate components.

works bridging hollows between sand grains are shown in Figure 10; this micrograph suggests that the network interstices were originally occupied by either sand grains or water. The small particles were stable in the electron beam, surviving for minutes with no apparent damage, whereas the gel network was not stable and the electron beam appeared to destroy the gel threads (by dehydration) after prolonged exposure.

The gel network exhibited smooth surfaces at early stages of formation (Figure 11A). The gel materials appear to have grown outward from the grain surfaces, forming branches and a network texture, similar to those observed in the formation of imogolite from pla-

https://doi.org/10.1346/CCMN.1989.0370304 Published online by Cambridge University Press

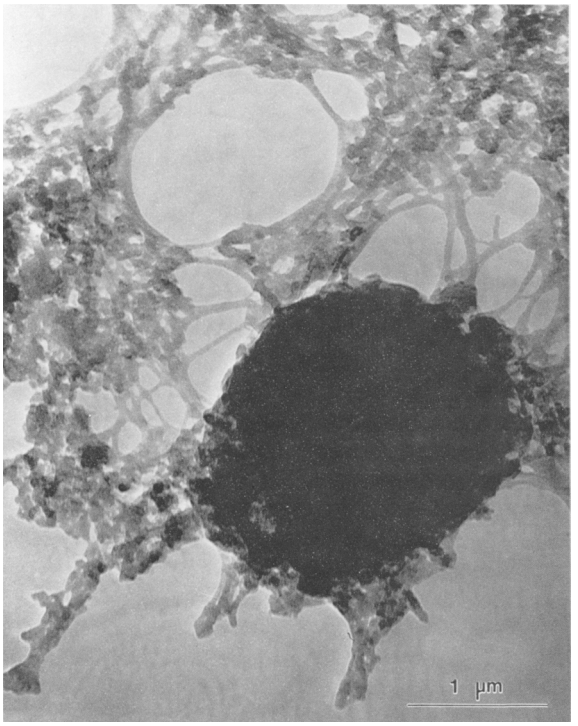

Figure 10. Transmission electron micrograph of gel cementing material showing networks bridging hollows and sand grains.

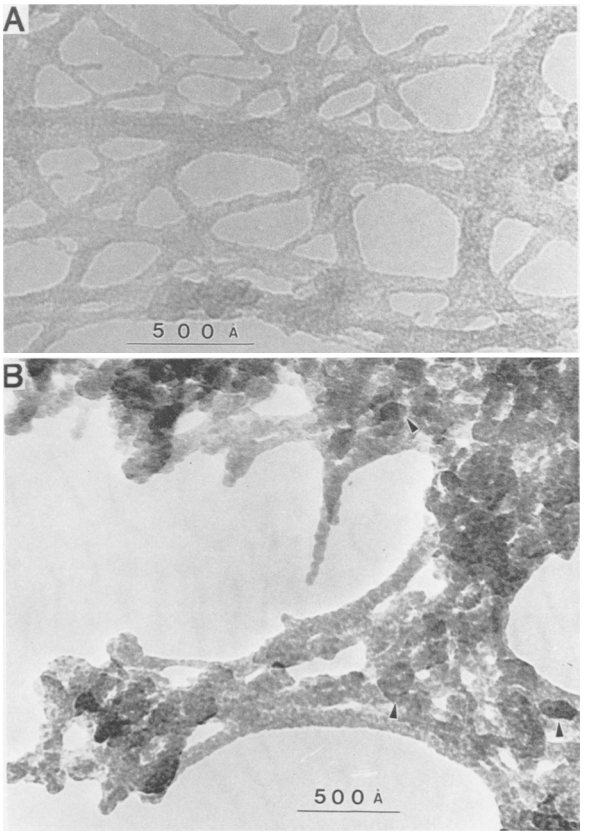

Figure 11. Transmission electron micrographs of (A) gel cementing material and (B) small particles on networks. Arrows indicate solitary particles.

gioclase grains in volcanic ash (Tazaki, 1979, 1980). Small platy particles appear to have formed on the network following its construction. The small, platy particles were either solitary, with generally poorly defined outlines, or coalesced (Figure 11B). The solitary particles (<200-Å in diameter) were thick and dense (arrows in Figure 11B). Commonly, two or more particles were coalesced. A few, well-preserved particles were hexagonal, although the morphology of most of the solitary particles was irregular.

The SAD pattern of the gel material lacked spots or rings (Figure 12b), whereas the small particles showed diffuse rings at 14.9, 9.4, 7.2, 5.1, 4.60, and 4.02 Å (Figure 12a). High magnification of regions between particles revealed the existence of crystalline or poorly ordered domains having 14–16-Å d-values. The spacings measured with TEM were similar to those found in the XRD pattern of the bulk sample.

EDX revealed that both the gel materials and the particles contained substantial Al and Si and traces of Cl, Ca, and Fe (Table 2). The gel materials showed slightly higher Al/Si ratios (2.2) than the particles (2.0). The Fe/Al ratio of the particles was 0.02. The noncrystalline gel networks appear to have transformed to a layered aluminosilicate structure.

The morphology of the small particles was similar to those observed in synthetic aluminosilicates that show broad 8.8- and 3.3-Å XRD peaks (Wada *et al.*, 1988), but the Al/Si ratio was quite different. The Al/Si ratio (2.0) and the d-value of the particles were similar to those of imogolite, but the morphology was different.

The TEM of the sample from which organic matter had been removed by H_2O_2 treatment (Figure 3) is shown in Figure 13. This treatment changed the organic matter to granular particles, which produced broad electron diffraction rings at 3.3, 2.7, and 1.8 Å (Figure 13). The XRD and the TEM results suggest the presence of clay-organic complexes, rather than imogolite in the cementing materials.

DISCUSSION

The cementing materials in the sand dune were characterized by poorly crystalline small particles and noncrystalline gel networks that were composed of an aluminosilicate having a high carbon content. On the basis of morphology, chemistry, and structure, the cementing materials appeared to be distinct from imogolite, kaolin-group minerals, or other oxides. The d-values of 14–16 Å, measured with XRD, TEM, and electron diffraction, suggest that the gel materials transformed to phyllosilicate particles. The Al/Si ratios of the gel

https://doi.org/10.1346/CCMN.1989.0370304 Published online by Cambridge University Press

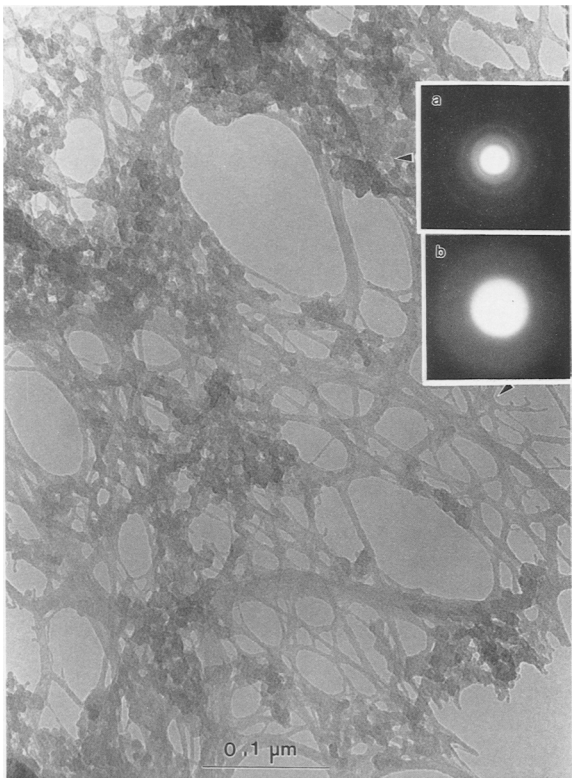

Figure 12. Selected-area electron diffraction patterns of gel material showing noncrystalline structure (b) and the small particles having diffuse rings at about 14.9, 9.4, 7.2, 5.1, 4.60, and 4.02 Å (a).

networks and the small particles are 2.2 and 2.0, respectively. The hydrocarbon content decreased markedly with an increase in depth into an individual particle, whereas the Al/Si ratio increased with depth. XPS showed three binding energies that were identified as CH_2, C–NH_2, and CO_3, suggesting that aluminosilicate, hydrocarbon, amine, and carbonate are present as a clay-organic complex, which constitutes the gel cementing agent.

Table 2. Chemical microanalyses (atom %) of gel materials and particles using transmission electron microscopy equipped with energy dispersive X-ray spectrometer.

	Gel		Particles	
	A	B	A	B
AlKα	63.10	67.00	64.87	64.66
SiKα	28.58	29.68	31.57	32.55
ClKα	1.86	0.00	1.41	0.57
CaKα	0.00	0.63	0.66	0.68
FeKα	6.46	2.69	1.48	1.54
Total	100.00	100.00	99.99	100.00
Al/Si	2.21	2.26	2.05	1.99
Fe/Al	0.10	0.04	0.02	0.02

A = at 150-Å depth; B = no sputter.

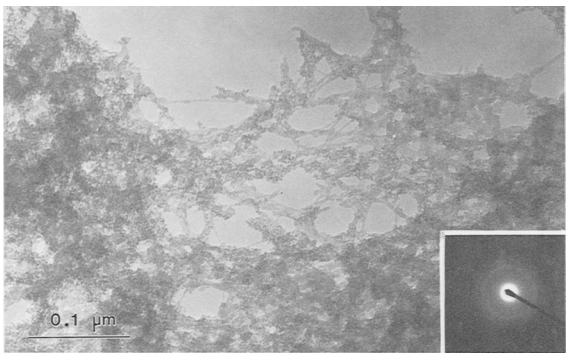

Figure 13. Transmission electron micrograph for gel cementing material from which organic matter was removed by treatment with H_2O_2, showing granular particles having broad 3.3-, 2.7-, and 1.8-Å electron diffraction rings.

The formation of clay minerals (i.e., imogolite and kaolin-group minerals) can be influenced by organic acids, citric acid, and polygalacturonate (Huang and Violante, 1986; Wada, 1977; Farmer, 1981; Ross and Kodama, 1979). These authors showed that in volcanic ash soil, A1 horizons rich in humus do not contain allophane or imogolite, whereas the B horizons without humus contain allophane and imogolite (Wada, 1980). Organic matter that migrated from the upper to the lower horizons of the dune may also be adsorbed by existing clay minerals. Organic acids, such as tannic, malic, and tartaric acids, disturb the formation of imogolite and allophane (Inoue and Huang, 1986). Organic acids can form surface chelates with alumina, and organic anions are specifically adsorbed by aluminum hydroxides (Nagarajah *et al.,* 1970). Thus, the behavior of organic matter in the sand dune may have controlled the formation of clay-organic complexes as the cementing agent.

Wada *et al.* (1988) synthesized five groups of aluminosilicates that have a close structural relation with allophane and imogolite. Their group V products consisted of large granules having diameters of >100 Å. The IR spectra of these materials resembled those of "hydrous feldspathoids" (Si/Al molar ratios >1.0) formed from alkaline solutions, similar to those found in the present study. None of the five groups of the synthesized products, however, contained a gel network. The gel cementing materials in the Arahama sand dune may therefore have been formed from biochemical weathering products of organic matter, which subsequently controlled the formation of clay-organic complexes.

ACKNOWLEDGMENTS

The authors are grateful to R. Humphrey (University of Guelph) and the staff at Surface Science Western for their help with the chemical analysis, and to H. Kodama (Agriculture Canada) for his advice.

REFERENCES

Berthelin, J. and Munier-Lamy, C. (1983) Microbial mobilization and preconcentration of uranium from various rock materials by fungi: *Ecol. Bull.* **35,** 395–401.

Bond, R. D. and Harris, J. R. (1964) The influence of the microflora on the physical properties of soils. I. Effects associated with filamentous algae and fungi: *Aust. J. Soil Res.* **2,** 111–122.

Clark, D. T., Cromarty, B. J., and Dilks, A. (1978) A theoretical investigation of molecular core binding and relaxation energies in a series of oxygen-containing organic molecules of interest in the study of surface oxidation of polymers: *J. Polymer Science,* Polymer Chem. Ed. **16,** 3173–3184.

Farmer, V. C. (1981) Possible roles of a mobile hydroxyaluminum orthosilicate complex (proto-imogolite) and other hydroxyaluminum and hydroxy-iron species in podzolization: in *Migrations Organo-Minerales dans les Sols Tempères,* Colloq. Int. CNRS no. 303, 1979, Nancy, France, Centre National de la Recherche Scientifique, Paris, 275–279.

Huang, P. M. and Violante, A. (1986) Influence of organic acids on crystallization and surface properties of precipitation products of aluminum: in *Interaction of Soil Minerals with Natural Organics and Microbes,* P. M. Huang and M. Schnitzer, eds., Soil Science Society of America, Madison, Wisconsin, 159–221.

Inoue, K. and Huang, P. M. (1986) Influence of selected organic ligands on the formation of allophane and imogolite: *Soil Sci. Soc. Amer. J.* **50,** 1623–1633.

Nagarajah, S., Posner, A. M., and Quirk, J. P. (1970) Competitive adsorption of phosphate with polygalacturonate and other organic anions on kaolinite and oxide surfaces: *Nature (London)* **228,** 83–84.

Niigata Ancient Dune Research Group (1967) Ancient dunes along the coast of the Japan Sea: *Quaternary Res.* **6,** 19–28.

Research Group of Harden Soil (1984) Characterization of the harden sand layer in Omiya, Japan: *Earth Science (Chikyū kagaku)* **38,** 17–30.

Ross, G. J. and Kodama, H. (1979) Evidence for imogolite in Canadian soils: *Clays & Clay Minerals* **27,** 297–300.

Spyridakis, D. E., Chester, G., and Wilde, S. A. (1967) Kaolinization of biotite as a result of coniferous and deciduous seedling growth: *Soil Sci. Soc. Amer. Proc.* **31,** 203–210.

Tazaki, K. (1979) Scanning electron microscopic study of imogolite formation from plagioclase: *Clays & Clay Minerals* **27,** 209–212.

Tazaki, K. (1980) Imogolite formed on weathered plagioclase: in *Electron Micrographs of Clay Minerals,* T. Sudo, S. Shimoda, H. Yotsumoto, and S. Aida, eds., Kodansya, Tokyo, 197–199.

Tazaki, K., Lindenmayer, Z. G., and Fyfe, W. S. (1988) Formation of ultra-thin Cu-S films on minerals: A weathering product from silicate-facies iron formation, Salobo, Carajas, Brazil: *Chem. Geol.* **67,** 285–294.

Wada, K. (1977) Allophane and imogolite: in *Minerals in Soil Environments,* J. B. Dixon and S. B. Weed, eds., Soil Science Society of America, Madison, Wisconsin, 603–638.

Wada, K. (1980) Mineralogical characteristics of Andisols: in *Soils with Variable Charge,* B. K. G. Theng, ed., New Zealand Soc. Soil Sci., Lower Hutt, New Zealand, 87–90.

Wada, K., Wilson, M., Kakuto, Y., and Wada, S. (1988) Synthesis and characterization of a hollow spherical form of monolayer aluminosilicate: *Clays & Clay Minerals* **36,** 11–18.

(Received 30 August 1988; accepted 24 November 1988; Ms. 1823)